

PAPER



Cite this: *New J. Chem.*, 2022, 46, 250

Synthesis of the new analogs of morpholine and their antiplasmodial evaluation against the human malaria parasite *Plasmodium falciparum*†

Charu Upadhyay,^a Neha Sharma,^b Sumit Kumar,^a Prem Prakash Sharma,^b Diana Fontinha,^c Bhupender S. Chhikara,^d Budhaditya Mukherjee,^{id e} Dhruv Kumar,^{id f} Miguel Prudencio,^{id c} Agam P. Singh^{id g} and Poonam^{id *a}

A series of morpholine analogs functionalized with hydroxyethylamine (HEA) pharmacophore was synthesized and assayed for the initial screening against *Plasmodium falciparum* 3D7 in culture, which suggested that analog **6k** is a hit molecule with an inhibitory concentration of $5.059 \pm 0.2036 \mu\text{M}$. Listed analogs were also assessed for toxicity against liver cells, HepG2, and none of them showed cytotoxicity up to 2 mM. Further, we tested all the compounds against a validated target, plasmepsin X, and the results were supported with molecular docking and molecular dynamic simulation. Overall, these novel compounds demonstrated moderate antiplasmodial activity without any toxic effects, and therefore medicinal chemistry optimization is essential to obtain analogs with improved biological activity.

Received 2nd September 2021,
Accepted 4th November 2021

DOI: 10.1039/d1nj04198c

rsc.li/njc

1. Introduction

Malaria disease, caused by *Plasmodium*, is one of the most life-threatening diseases affecting 200 million people worldwide, especially in tropical and sub-tropical regions.^{1,2} Among the *Plasmodium* species, *Plasmodium falciparum* (Pf) is the most lethal form of human malaria.^{3,4} According to a WHO report, a decrement in the mortality rate has been observed since 2011 as the number of deaths reduced from 536 000 to 40 900 in 2019.⁵ In sub-Saharan countries, the front-line therapeutics, *i.e.* quinolines, naphthoquinones, antifolates, 8-aminoquinolines, endoperoxides and artemisinin-based combination (ACT) are available to treat the disease.⁶ Regardless of uninterrupted

events towards disease control, inevitable drug resistance has emerged as a major barrier, and thus efforts are necessary to overcome the problem of the decreased efficacy of therapeutics.^{7,8} However, ACT treatments remain the most effective therapy for malaria disease.^{9,10} The efficacy of the drugs is compromised at any stage of their life, probably due to their frequent and suboptimal doses,^{11,12} and ACT resistance is emerging in malaria cases reported along the border of Cambodia.^{3,13,14} Considering the current alarming circumstances, it is necessary to design new, potent, and effective antimalarial drugs, preferably active beyond the asexual blood-stage of malaria.¹⁵

The development of novel chemical libraries based on the validated pharmacophores and their screening against malaria parasites remains one of the potential approaches to finding hit molecules. Looking at the significance of the heterocyclic scaffolds, morpholine analogs have been investigated as high-valued bioactive scaffolds, utilized as potential synthons in medicinal chemistry. Various morpholine analogs have been studied as antioxidants, anti-inflammatory, antimicrobial, analgesics, and anti-cancer agents.^{16–19} Moreover, morpholine is an integral part of various drug molecules where it acts as an enzyme active-site inhibitor for enzymes such as phosphatidylinositol 3-kinase, squalene synthase, peptidyl transferase, *etc.*, and contributes to favorable pharmacological applications.²⁰ Notably, two well-known antimalarials, namely M5717 and OZ439, containing a morpholine core are under clinical trials,^{6,21} indicating their suitability as important pharmacophores for the

^a Department of Chemistry, Miranda House, University of Delhi, Delhi, India.
E-mail: poonam.chemistry@mirandahouse.ac.in

^b Laboratory for Translational Chemistry and Drug Discovery, Department of Chemistry, Hansraj College University Enclave, University of Delhi, Delhi 110007, India

^c Instituto de Medicina Molecular, Faculdade de Medicina, Universidade de Lisboa, Avenida Professor Egas Moniz, 1649-028 Lisboa, Portugal

^d Department of Chemistry, Aditi Mahavidyalaya, University of Delhi, Delhi, India

^e School of Medical Science and Technology, IIT Kharagpur, Kharagpur-721302, India

^f Amity Institute of Molecular Medicine & Stem Cell Research, Amity University Uttar Pradesh, Noida, India

^g Infectious Diseases Laboratory, National Institute of Immunology, Aruna Asaf Ali Marg, New Delhi 110067, India

† Electronic supplementary information (ESI) available. See DOI: 10.1039/d1nj04198c

design of novel antimalarial drugs. Hydroxyethylamine (HEA) has also been validated as a potential pharmacophore for antimalarial drug discovery.^{22,23} Our group has explored many HEA compounds as highly effective against multiple life stages of the malaria parasite (*i.e.*, liver stage, blood stage, and sexual stages), and have ultimately suggested them as multistage antimalarial compounds.^{24,25} Interestingly, the efficacy of HEA compounds can be easily tuned with the inclusion of high-valued heterocyclic scaffolds.

Subsequently, we designed and synthesized novel morpholine-based HEA compounds anticipating them as potent antiplasmodial agents not only against blood-stage but also liver-stage infection. Being important pharmacophores, the fusion of HEA and morpholine could increase the efficacy parameters and structural diversity. All the fourteen listed compounds were screened against blood-stage and liver-stage activity. Additionally, compounds were evaluated against recombinant Plm X and the results were substantiated with extensive *in silico* studies.

2. Results and discussion

2.1. Compound synthesis

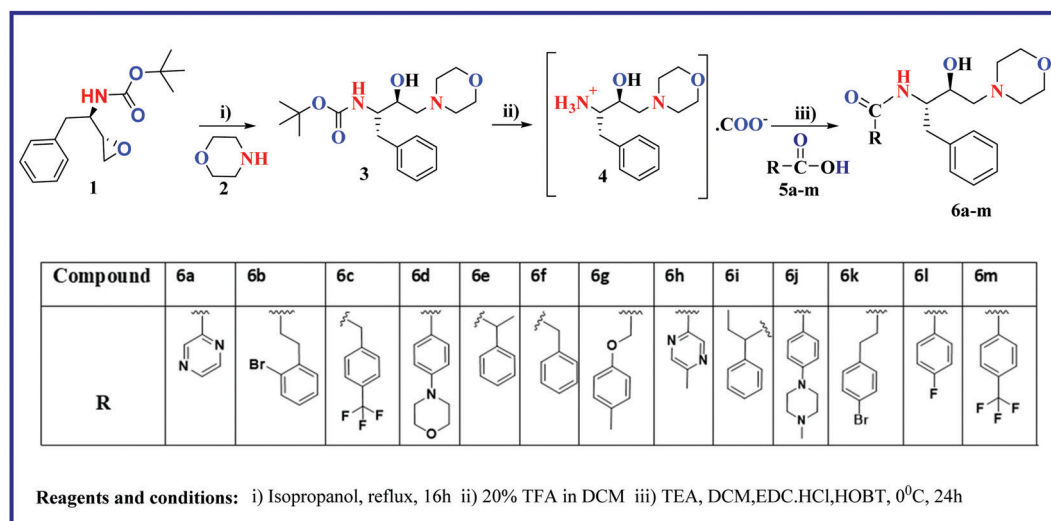
The design of novel compounds based on validated pharmacophores remains one of the important paths to discovering efficacious therapeutics. In this manuscript, we present the fusion of two important and validated pharmacophores, *i.e.*, morpholine and HEA, which have led to fourteen new compounds possessing chemical diversity. In the literature, HEA analogs decorated with various heterocyclic scaffolds have been widely studied as inhibitors of malarial aspartyl proteases, Plms,²⁶ and as potential multistage antimalarials.^{9,27} Likewise, the morpholine scaffold was explored for medicinal applications including antimalarial drugs.²⁸ Encouraged by this, we designed novel compounds based on morpholine and HEA, which were assessed for ADME profile predictions using the SWISS-ADME

server. All molecules strictly obey the Lipinski rule of five, where $MW < 500$, $AcptHB < 10$, $DonorHB < 5$, $MlogP < 4.15$. There is no violation for any single parameter of Lipinski drug-like characteristics among all synthesized analogs. All the molecules have high GI absorption, while **3**, **6b-c**, **6e-f**, **6i**, **6k-m** were the only molecules displayed blood-brain barrier (BBB) penetration capabilities. Molecules are moderately soluble having $\log S$ of -4.00 , soluble (range -4.00 to -2.00), and very soluble (0 to -2.00). Subsequently, the syntheses of fourteen HEA and morpholine-based derivatives were performed by following a simple and convenient method as illustrated in Scheme 1. To obtain structural activity relationship (SAR) insights, chemical diversity was introduced in the desired compounds by embodying aromatic and heterocyclic rings possessing fluorine, bromine, trifluoromethyl, and methyl groups. Our group²⁹⁻³¹ has already optimized a facile, rapid, and regioselective^{32,33} ring-opening of epoxide, (*2R,3S*)-3-(*N*-BOC-amino)-1-oxirane-4-phenylbutane with different amines with inversion of the configuration at less hindered carbon atom. The same synthetic route was implemented using morpholine as the amine, which resulted in the Boc-protected intermediate (**3**). In the next step, deprotection of **3** was carried out, followed by the coupling reaction with functionalized aromatic carboxylic acids, which afforded the final desired compounds (**6a-m**).^{34,35}

New compounds were obtained in moderate to good yields. The chemical structure of all the listed compounds was confirmed by NMR (¹H & ¹³C) and mass spectrometry.

2.2. Biological evaluation

2.2.1. Antiplasmodial growth inhibition assay, cytotoxicity evaluation, and hemolysis assay. All the newly synthesized compounds (**3**, **6a-m**) were tested for their antiplasmodial activity on an asynchronous culture of the chloroquine-sensitive strain Pf3D7 at concentrations of 1 and 10 μ M (Fig. S33, ESI[†]) with ART as the positive control. One complete intraerythrocytic growth cycle of *Pf* was examined post-treatment.



Scheme 1 Synthesis of HEA-morpholine compounds (**6a-m**).

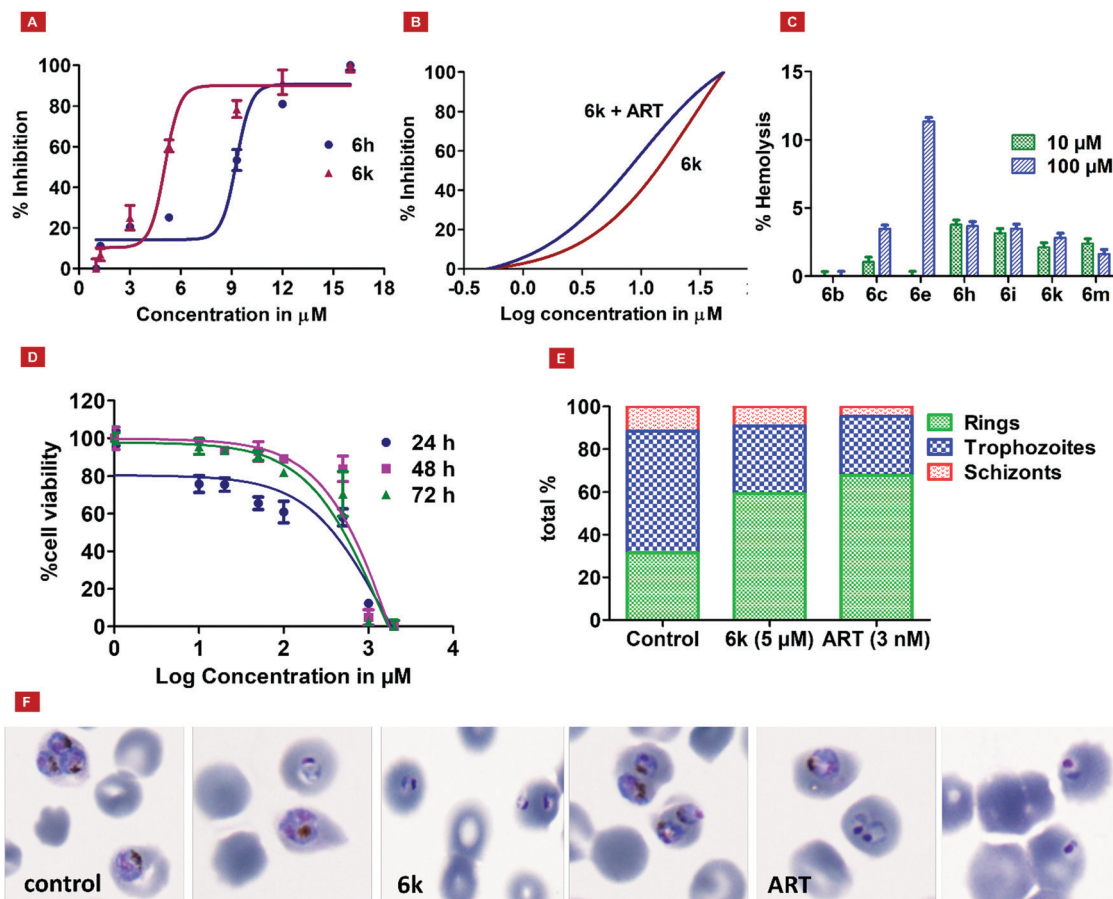


Fig. 1 The efficacy and cytotoxicity effects of compounds. (A) The effects of dose-dependent ABS (asexual blood-stage) of compound **6h** and **6k** on *Pf3D7* strains in culture. An asynchronized parasite population of *Pf3D7* infected erythrocytes (4% final hematocrit and 1% parasitemia) was exposed to varying concentrations of test compound **6h** and **6k**. (B) Two different curves showing the % inhibition of compound **6k** alone (red curve) and in combination with ART (blue curve). (C) The effects of the compounds on human RBCs at 10 μM and 100 μM concentrations. (D) Cell viability (%) levels were measured by MTT assay after 24, 48, and 72 h of treatment at different concentrations (1 μM to 2 mM). (E) The percentages of rings, trophozoites, and schizonts in the control, treated (**6k**), and ART at their IC_{50} values in the trophozoite stage of the malaria parasite. (F) Photomicrographs of Giemsa-stained blood smears of the control (3.6% parasitemia), **6k**, and ART on the trophozoite stage of the parasite morphological appearance.

The Giemsa-stained blood smear method was employed to measure the percentage growth inhibition of the parasite. The parasitemia in control was 3.6% after 48 hrs (without DMSO) and the positive control taken was ART (1 μM), which showed $\sim 98\%$ inhibition. Four of the compounds, **6e**, **6f**, **6h**, and **6m** displayed moderate inhibitory effects ($> 50\%$ inhibition) at 10 μM concentration, however, **6k** showed $> 80\%$ inhibition. Further, the screening results of **6h** and **6k** in replicates suggested that these compounds inhibited *Pf* growth in a dose-dependent manner, *i.e.*, the growth percentage decreased with an increase in the concentration of the compounds. The 50% inhibitory concentration (IC_{50}) values of **6h** and **6k** were determined and noted as 9.3 ± 0.2 and 5.0 ± 0.2 μM , respectively (Fig. 1A).

To evaluate the cytotoxicity of all the listed compounds, an MTT assay was performed against HepG2 (a mammalian liver cell line). The minimal cytotoxic effect was shown by **3**, **6a**, **6h**, and **6j** with $\text{TC}_{50} > 2$ mM. In a separate experiment, all the synthesized compounds were tested on normal human red blood cells (RBCs), to find the hemolysis of RBCs at two different concentrations, *i.e.*, 10 μM and 100 μM . Results are

shown in Fig. 1C. Interestingly, no significant lysis of RBCs was found up to the 100 μM concentration. We also performed time course dose-dependent cytotoxicity experiments for hit **6k** and evaluated its TC_{50} at different time intervals, *i.e.*, 24, 48, and 72 hours at different concentrations ranging from 1 μM to 2 mM. The results showed tolerance for hit **6k** with TC_{50} values of 179.9, 496.2, and 383.3 μM at 24, 48, and 72 hours, respectively (Fig. 1D).

2.2.2. In vitro drug combination assay. To evaluate the combined effect of **6k** and ART, a growth inhibition assay was performed for **6k** alone (0.5 μM , 5 μM , 50 μM) and in combination with ART (0.5 nM). Synchronized culture was used and treated for 48 hours. The results of combination studies were found to be better than the individually treated compound. The compound showed a synergistic effect with ART, as its IC_{50} value decreased when combined with ART at a fixed dose (0.5 nM) as shown in Fig. 1B.

2.2.3. Stage-specific study in the blood stage. Stage-specific profiling of **6k** was performed using a synchronized culture of the *Pf3D7* strain. Here, **6k** and ART (positive control) treatments

Table 1 Structures of all the synthesized analogs with their melting points, yields, TC₅₀, and % inhibition against PlmX and Pf3D7

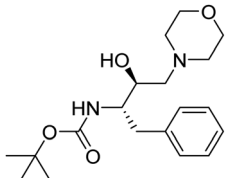
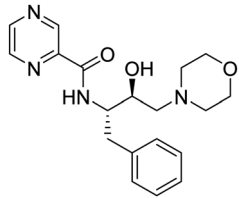
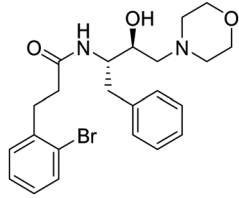
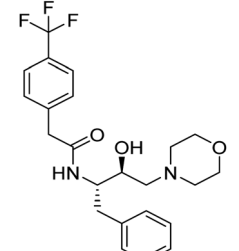
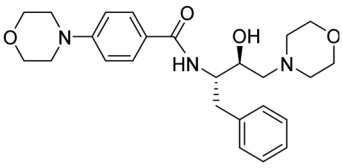
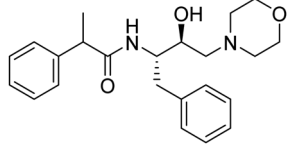
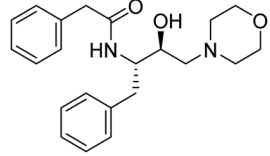
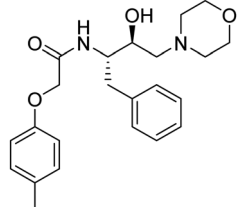
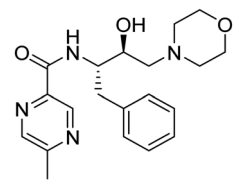
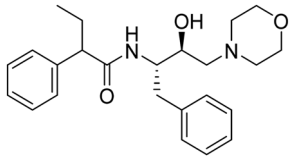
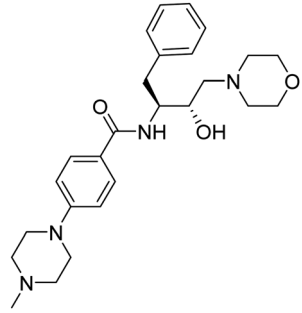
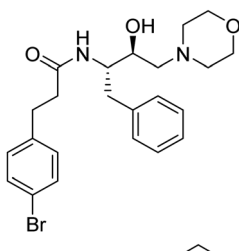
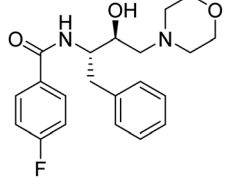
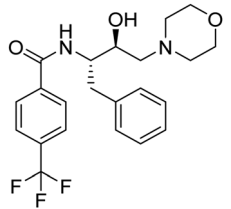
Entry no.	Code	Structure	TC ₅₀ (HepG2)	% reduction of PlmX activity at 1 μM	% inhibition of Pf3D7 at 10 μM
1.	3		> 2 mM	10.9375	40.64
2.	6a		> 2 mM	11.29167	45.74
3.	6b		486 μM	10.10417	48.61
4.	6c		200 μM	28.89583	40.47
5.	6d		> 900 μM	14.1875	45.19
6.	6e		> 1350 μM	11.6875	51.89
7.	6f		> 900 μM	16.875	53.26
8.	6g		1350 μM	15.52083	44.59

Table 1 (continued)

Entry. no.	Code	Structure	TC ₅₀ (HepG2)	% reduction of PlmX activity at 1 μM	% inhibition of Pf3D7 at 10 μM
9.	6h		> 2 mM	38.41667	51.73
10.	6i		683 μM	12.8333	34.67
11.	6j		> 2 mM	13.95833	45.07
12.	6k		233 μM	30.39583	84.17
13.	6l		> 1350 μM	24.75	47.54
14.	6m		1032 μM	22.72917	55.13

were done on the trophozoite stage as this stage is crucial for various protein syntheses at their respective IC₅₀ values of 5 μM and 3 nM, respectively, as shown in Fig. 1E. After 50 hours of incubation, the percentages of different stages (rings, trophozoites, and schizonts) were counted and captured. In the control (3.6% parasitemia), a healthy life cycle was observed (31.5% rings, 56.9% trophozoites, 11.5% schizonts), whereas, upon treatment with **6k** (59.3% rings, 31.5% trophozoites, 9.1% schizonts), a decrease in the percentage of trophozoites was

observed. As per the literature, ART was found to be more active at the trophozoite stage rather than the mid-ring-stage parasite,³⁶ which supports our results as ART (67.8% rings, 27.4% trophozoites, 4.6% schizonts) displayed a delay in the different stages of the parasite (significantly trophozoites). When compound **6k** and ART were treated at their IC₅₀ values, *i.e.*, 5 μM and 3 nM, respectively, we noticed that the maximum efficacy for **6k** was attained when treatment was done at the trophozoite stage. This reflects the action of compound **6k** at

the protein synthesis stage, which is crucial for the parasite survival.³⁷

2.2.4. *In vitro* activity against *P. berghei* hepatic (liver) stage. Despite its asymptomatic behavior, the liver stage of the malaria parasite is a crucial phase for the development of effective drugs since it leads to the release of thousands of parasite-filled vesicles, known as merozoites into the blood.³⁸ This phenomenon causes blood infection, known as the erythrocytic stage. Consequently, in order to eliminate the infection in the early stage, intervention during the liver stage is mandatory. However, very few existing drugs (*i.e.*, atovaquone and pyronaridine) are known to treat the liver stage infection, which warrants further discovery of more such effective drugs.^{39,40} We assessed our compounds against the liver stage of the parasite in culture. During the screening, *P. berghei* infection was produced in Huh7 cells and then treated with the compounds at two concentrations, 1 and 10 μM . Primaquine (PQ) was included as a positive control, whereas DMSO served as the negative control. Unfortunately, no promising results were observed in the initial screening as none of the compounds showed more than 50% inhibition at 10 μM , and therefore we did not proceed further for IC_{50} determinations. Since aliphatic linkers are necessary for the activity of molecules in the liver stage, the insertion of alkyl chains into these moieties could show inhibition in the liver stage.^{41,42}

2.2.5. Plasmepsin X inhibition assay and *in silico* studies. Malarial aspartyl proteases, plasmepsins (Plms), have been considered as promising targets for the development of antimalarial drugs because of their crucial role in providing nutrients to the growing parasite in all the life stages of the parasite.⁴³ In recent years, Plm X emerged as one of the potential drug targets over the other Plms.^{44,45} Merozoites use Plm X to invade fresh RBCs in order to continue the parasite life cycle.⁴⁶ It has been observed that the secondary hydroxyl group in HEA mimics the geometry of the Plms active site and blocks it from entering into another phase of the life cycle of the parasite.⁴⁷ HEA-based molecules inhibit the active sites of Plm and hence, block the further degradation of hemoglobin.⁴⁸ Contributing to this, morpholine-linked moieties are also under clinical and pre-clinical trials, showing their potential as antimalarial compounds.^{37,49} Based on these facts, a Plm X inhibition assay was performed since this protein is known as a potential target due to its presence in all the life stages of the malaria parasite, and inhibitors against this protein could be important tools for malaria elimination. Also, the previously reported compound **49c** displayed multistage inhibition of Plm IX and PlmX in the nanomolar range.^{25,50} In this study, recombinant *Pf*Plm X activity was assessed for all the listed HEA-morpholine-based analogs.⁴³ The % reduction of Plm X activity at 1 μM concentration was evaluated and the results are shown in Table 1. Among fourteen compounds, **6h** and **6k** displayed good % inhibition of 38.41 and 30.39, respectively (Table 1, entry 9 and 12), at 1 μM . Subsequently, compound **6h** was selected for K_i value determination and it was noted as 1.015 μM .

The developed Plm X model (Fig. S34A, ESI[†]) was analyzed for its stereochemical geometry by the ProCheck Ramachandran plot. The amino acid residues (Glu_204 and Gln_238), which were found to be in the outlier region, contributed only 0.7% of the total, indicating good structural geometry for the complex. Residues lying in favored, additionally allowed, and generously allowed regions were 87.7%, 11.2%, and 0.4%, respectively (Fig. S34B, ESI[†]). *In silico* studies revealed that **6h** displayed the best parameters such as docking score, XP Gscore, and binding free energy with the values of -6.12 , -6.802 , and -79.6 kcal mol⁻¹, respectively (Table 2, entry 1). However, **6k**, the most potent molecule in the asexual blood stage, was found to possess a docking score, XP Gscore, and binding free energy of -5.216 , -5.891 , and -69.26 kcal mol⁻¹, respectively (Table 2, entry 10), in correlation with the anti-proliferative effect against *Pf* as discussed in the previous sections. The molecular docking analysis indicated that the hydroxyl group and phenyl moiety of HEA interacted with residues Asp_266 and Phe_311 through H-bond and pi-pi interactions, respectively. The nitrogen atom of the morpholine moiety showed interactions with Asp_266 and Phe_311 *via* the salt bridge and pi cation interactions, respectively (Fig. 2).

The amino acid residue Asp_266 is a known catalytic residue of Plm X and interestingly, the hit molecule (**6k**) showed interaction with the same. Therefore, to further analyze the binding and conformational stability of (**6k**) with PlmX protein, molecular dynamics (MD) simulation studies were performed.

Firstly, the stereochemical geometry analysis was carried out after performing MD simulation for 50 ns using the Ramachandran plot, which revealed acceptable numbers of residues in the favored, additionally allowed, and generously allowed regions of 81.5%, 17.0%, and 1.1%, respectively. The complex was observed to have only one residue (Asp_518) in the outlier region of the Ramachandran plot (0.4%) (Fig. S34C, ESI[†]). Overall, the complex showed a sterically acceptable conformation of their receptor Plm X protein molecule after the MD simulation study, indicating the complex to be stable in nature.

Next, the binding behavior of the **6k**-Plm X complex was analyzed. The Root Mean Square Deviation (RMSD) of the C α of the Plm X protein was analysed during the 30 ns simulation of

Table 2 Molecular docking results for the HEA-morpholine series of compounds

Entry	Compound	Docking score	XP GScore	MMGBSA dG Bind
1	6h	-6.12	-6.802	-79.6
2	6e	-5.892	-6.115	-57.37
3	6j	-5.65	-6.343	-64.89
4	6b	-5.492	-5.721	-61.69
5	6g	-5.46	-6.191	-56.83
6	6m	-5.432	-5.68	-50.82
7	6i	-5.425	-6.11	-60.88
8	3	-5.298	-6.016	-64.68
9	6f	-5.283	-5.506	-45.62
10	6k	-5.216	-5.891	-69.26
11	6d	-4.872	-5.508	-59.89
12	6c	-4.846	-5.529	-62.68
13	6a	-4.771	-5.453	-66.15
14	6l	-4.68	-4.928	-38.2

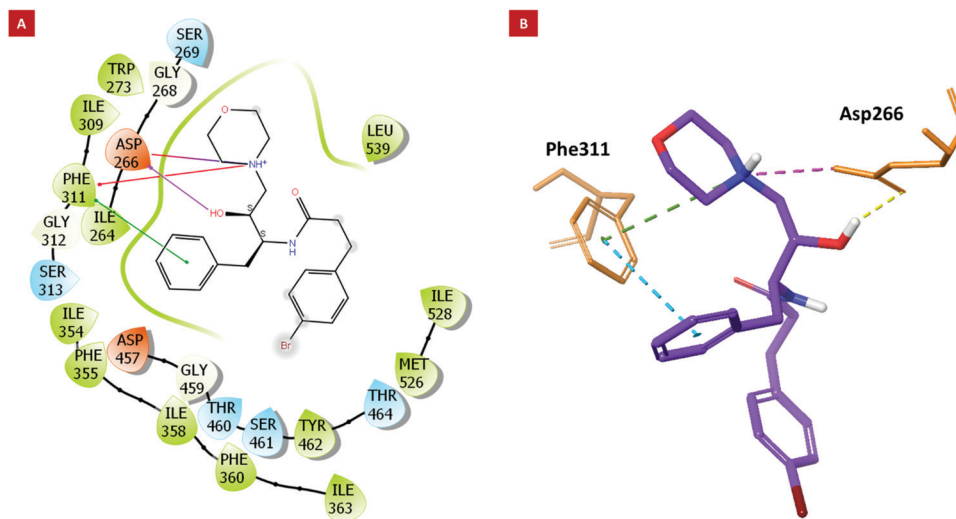


Fig. 2 Molecular docking results. (2A) The 2D and (2B) 3D interaction images of **6k** with key residues of PlmX.

the **6k**–PlmX complex. The RMSD plot indicated that the **6k**–PlmX complex reached its stable conformation within the first few nanoseconds and maintained its stability till the end of the simulation (Fig. 3). The C α RMSD of Plm X attained the plateau phase within the first 5 ns of simulation time, where average C α RMSD was observed as 3.45 Å. The stability of ligand RMSD can be viewed in Fig. 3, where an average RMSD of **6k** was found as 3.08 Å. The RMSD of both protein C α and the ligand fluctuated within an acceptable range (3 Å).

The Asp266 residue interacted with both the nitrogen atoms of the morpholine ring and the hydroxyl moiety of HEA by 75% and 88% *via* H-bond, respectively. The 2D interaction poses and the protein–ligand interaction histogram chart are shown in Fig. S35 (ESI[†]). The histogram showed favoured H-bond interactions with Asp_266; hydrophobic interactions with Ile264, Phe_311, Tyr357, Ile358, Phe360, Ile_363, Tyr_431, Met526, and Ile528; salt bridge with Asp_266, Asp_457, and water bridged interactions with Asp_266, Gly_268, Gly312, Ser313, Tyr357, Tyr_431, Asp_457, Gly459, The_460, and Arg534. Overall, these interactions facilitated **6k** structural and conformational stability within the binding pocket. The panels show the total number of specific contacts the PlmX protein made with **6k**

over the course of the simulation. The PlmX protein made 5–6 contacts with compound **6k** during the MD simulation (Fig. S34D, ESI[†]). The ligand–protein stable association would have contributed to the activity of compound **6k**.

2.2.6. Structure–activity landscape index similarity map of the synthesized morpholine HEA-based analogs (6a–m). Evaluation of the structure–activity landscape index (SALI) matrix of these novel morpholine-HEA compounds was performed using OSIRIS DataWarrior V 5.2.1 software (www.openmolecules.org). As shown in Fig. 4, the structure similarity relationship of the compounds was calculated based on the neighboring scaffolds with a similarity threshold greater than 84%. Introduction of a methyl linker at the *para* position of the pyrazine moiety in compound **6h** displayed better activity against *in vitro* Plm X (38.41% inhibition, Table 1, entry 9) as well as an asexual blood-stage (51% inhibition at 10 μ M against *Pf*3D7) when compared to the non-substituted pyrazine-containing

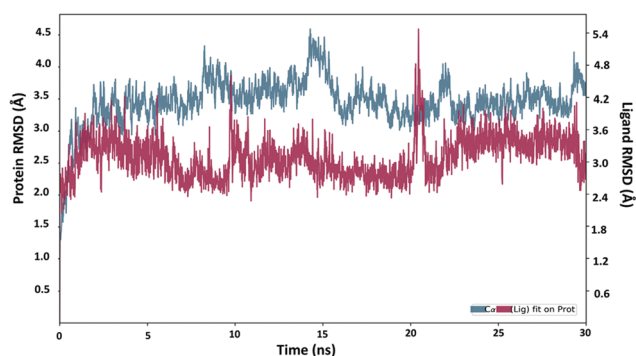


Fig. 3 The RMSD plot obtained for the **6k**–PlmX complex.

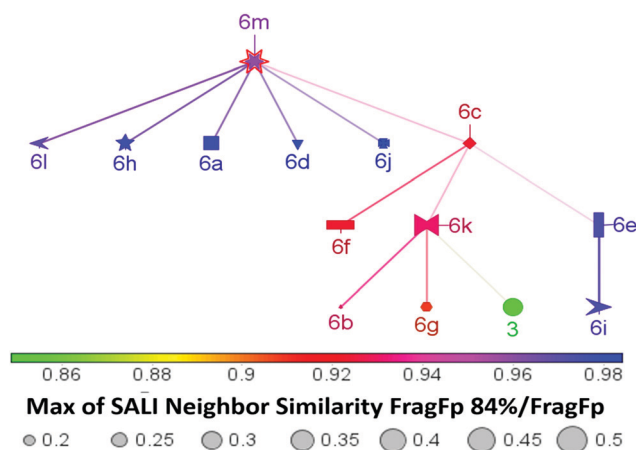


Fig. 4 Structure–Activity Landscape Index Similarity Map of the compounds. A scatter plot of the similarity relationships between antiparasitodal scaffolds based on the neighbour similarity FragFp-84% in a layered graph with the root at the top.

moiety, *i.e.*, **6a** (45% inhibition at 10 μM against *Pf3D7*). Replacement of the trifluoromethyl group (**6m**, 55% inhibition) by the fluorine group (**6l**, 47% inhibition) showed a moderate increment in the antiparasmodial activity. However, an increase in the carbon atom as in compound **6c**, (40% inhibition) led to a decrease in the activity. Moreover, the increase in carbon atoms by one methyl group in the phenyl ring did not show any significant change in activity (**6e**, 51% inhibition, and **6f**, 53% inhibition) but a further increment by two methyl groups (**6i**, 34% inhibition) resulted in lowered activity. Compound **6k**, having a bromine group at the *para* position of the phenyl ring showed better inhibition against *Pf3D7* in the asexual blood stage with an IC_{50} value of $5.0 \pm 0.2 \mu\text{M}$ as compared to molecule **6b** (48% inhibition) having a bromine group at the *ortho* position of the phenyl ring. Overall, it was concluded that **6k** was the most active against the *Pf3D7* strain of malaria in ABS but **6h** showed the maximum inhibition against the *in vitro* Plm X inhibition assay.

3. Conclusion

In this article, we have demonstrated the synthesis, *Pf3D7* activity, liver-stage activity, and PlmX activity of novel morpholine analogs. Although the compounds did not exhibit high potency against the malaria parasite, their tolerance up to 2 mM for normal cells combined with negligible lysis in RBCs up to 100 μM concentration were notable observations. Hit analog **6k**, possessing the 3,4-bromophenyl substituent also revealed significant activity against malarial aspartyl protease, PlmX, and the results were further supported by *in silico* studies, supporting the stability of the ligand within the binding pocket. From SAR analysis, it was noted that the presence of a bromine substituent at the *para* position of the phenyl ring showed improved antiparasmodial activity over the analog **6b** that holds bromine at the *ortho* position of the phenyl ring. Subsequently, medicinal chemistry optimization is essential to enhance the biological efficacy of **6k** and obtain lead compounds based on HEA-morpholine.

4. Experimental

4.1. General method

The chemicals and solvents used in the syntheses were obtained from commercial sources. Epoxide (2R,3S)-3-(N-BOC-amino)-1-oxirane-4-phenylbutane was purchased from GLR Innovation (New Delhi, India) and the carboxylic acids were purchased from TCI. The completion of the reaction and the purity of the final product were assayed by thin-layer chromatography (TLC). Small amounts of impurities left along with the product were further purified by column chromatography on alumina gel columns (100–200 mesh size, CDH). The melting points of the isolated compound were measured in open glass capillary tubes on a "BUCHI Labortechnik AG CH-9230". Nuclear magnetic resonance (NMR), ^1H , and ^{13}C spectra were recorded using a JEOL ECX-400P NMR Spectrometer using TMS as an internal standard. The splitting patterns were reported as

singlet (s), doublet (d), triplet (t), quartet (q), and multiplet (m). Further, a high-resolution Biosystems Q-Star Elite time-of-flight electrospray mass spectrometer was used for the characterization of the compounds. For HPLC analysis, an HPLC system (Gilson, USA) with an analytical column (C18), and a Thermo Separation Spectra SERIES UV100 detector coupled with software were used. The solvent used for the sample preparation for HPLC analysis was a mixture of acetonitrile and water.

4.2. General procedure

Epoxide **1** (1 eq., 19 mmol) and morpholine **2** (1 eq., 19 mmol) were dissolved in isopropanol and the reaction was refluxed for 16 h. The completion of the reaction was monitored by TLC. Later, the mixture was allowed to cool and the remaining solvent was evaporated under reduced pressure to obtain compound **3** as a white solid. Compound **3** was dissolved in dichloromethane (DCM), then 20% of trifluoroacetic acid (TFA) was added dropwise at 0 $^\circ\text{C}$ and the reaction mixture was stirred on a magnetic stirrer for 2 h to obtain intermediate **4**. After monitoring the TLC to ensure the completion of the reaction, DCM was removed under reduced pressure. In order to remove excess TFA, DCM was added and subsequently evaporated three times under vacuum. For the last step, **5a** (88 mg, 0.34 mmol) was dissolved in DCM (30 mL) and 1 mL of triethylamine (TEA) was added to it in a round-bottom flask, and the reaction was stirred for 20 minutes. After that, *N*-(3-dimethylaminopropyl)-*N'*-ethylcarbodiimide hydrochloride (EDC-HCl) (97 mg, 0.51 mmol) was added, followed by the addition of anhydrous 1-hydroxybenzotriazole (HOBT) (69 mg, 0.51 mmol) within a time gap of 20 minutes. To the reaction mixture, compound **4** (deprotected HEA) was added at 0 $^\circ\text{C}$ and stirred for 24 h at room temperature. The formation of the final product, **6a** was confirmed by TLC. The workup was done by removing the excess solvent under reduced pressure. The crude product was extracted using ethyl acetate and water as solvents. Traces of water were removed by treating the organic layer with anhydrous Na_2SO_4 . After evaporation, an oily product was obtained, which was further purified by column chromatography using alumina and ethyl acetate/hexane as eluents (10:90). The final compound **6a** was obtained as a white solid.

The above procedure was followed to synthesize compounds **6b–m** in fair yields (40–60%).

The structures of the compounds (**6a–m**) were confirmed by different spectroscopic techniques and the spectra have been provided in the ESI† (Fig. S1–S32).

4.2.1. Tert-butyl(3-hydroxy-4-morpholino-1-phenylbutan-2-yl)carbamate (3). White solid; m.p. 70–74 $^\circ\text{C}$; R_f value: 0.7 (1:9 methanol/chloroform). Yield: 99%. ^1H NMR (400 MHz, CDCl_3): δ 7.24–7.15 (m, 5H, $-\text{C}_6\text{H}_5$), 5.05 (d, $J = 9.5$ Hz, 1H, $-\text{OH}$), 3.69–3.63 (m, 8H, $2 \times \text{NCH}_2 + \text{OCH}_2$ of morph), 2.90–2.86 (m, 2H, $-\text{CH}_2$ -Ph), 2.53–2.51 (m, 2H, $-\text{CH}_2$ -morph), 2.39–2.37 (m, 1H, $-\text{CH}(\text{OH})\text{CH}_2$), 2.31 (brs, 1H, $-\text{NH}$), 2.22–2.20 (m, 1H, $-\text{NH}-\text{CH}$), 1.35 (s, 9H, $-(\text{CH}_3)_3\text{C}$). ^{13}C NMR (101 MHz, CDCl_3): δ 155.91 (s), 138.40 (s), 129.50 (s), 128.44 (s), 126.34 (s), 79.22 (s), 66.99 (s), 65.37 (s), 61.29 (s), 53.62 (s), 53.33 (s), 39.38 (s), 28.44 (s).

4.2.2. *N*-(3-Hydroxy-4-morpholino-1-phenylbutan-2-yl) pyrazine-2-carboxamide (6a). White solid; m.p. 157–160 °C; R_f value: 0.6 (1 : 9 methanol/chloroform). Yield: 58%. ^1H NMR (400 MHz, CDCl_3): δ 9.32 (s, 1H, *ortho*-NCH- of pyrazine), 8.71 (s, 1H, *para*-NCH- of pyrazine), 8.51 (s, 1H, *meta*-NCH- of pyrazine), 8.19–8.17 (d, $J = 9.5$ Hz, 1H, -NH-), 7.26–7.23 (m, 5H, -C₆H₅), 4.25–4.23 (d, $J = 9.3$ Hz, 1H, -OH), 3.83–3.79 (m, 1H, -CH(OH)CH₂-), 3.65–3.63 (m, 4H, 2x-OCH₂- of morph), 3.05–3.03 (d, $J = 7.7$ Hz, 2H, -CH₂-Ph), 2.97–2.95 (m, 1H, -CH-NH-), 2.56–2.53 (m, 2H, -CH₂-morph), 2.31–2.29 (m, 4H, 2x-NCH₂- of morph). ^{13}C NMR (101 MHz, CDCl_3): δ 162.96 (s), 147.38 (s), 144.53 (s), 144.39 (s), 142.75 (s), 137.80 (s), 129.48 (s), 128.62 (s), 126.67 (s), 66.73 (s), 65.23 (s), 61.48 (s), 52.15 (s), 39.02 (s), 29.78 (s). HRMS m/z calcd $[\text{M} + \text{H}]^+$ for C₁₉H₂₅N₄O₃⁺: 357.1926; found: 357.1916.

4.2.3. *N*-(1-Benzyl-2-hydroxy-3-morpholin-4-yl-propyl)-3-(2-bromo-phenyl) propionamide (6b). White solid; m.p. 125–128 °C; R_f value: 0.4 (1 : 9 methanol/chloroform). Yield: 52%. ^1H NMR (400 MHz, CDCl_3): δ 7.51–7.49 (d, $J = 7.9$, 1.0 Hz, 1H, -CH (*ortho*) of Br-C₆H₄-), 7.29–7.27 (d, $J = 6.5$ Hz, 1H, -CH (*meta*) of Br-C₆H₄-), 7.25 (d, $J = 1.5$ Hz, 1H, -CH (*para*) of Br-C₆H₄-), 7.22–7.16 (m, 5H, -C₆H₅), 7.06–7.02 (m, 1H, -CH (*meta*) of Br-C₆H₄-), 5.87–5.84 (d, $J = 9.4$ Hz, 1H, -OH), 4.06–4.00 (m, 1H, -CH(OH)CH₂-), 3.69–3.64 (m, 5H, 2x-OCH₂- of morph + -NH-CH-), 3.00–2.98 (m, 2H, -CH₂-(CO)-), 2.86–2.84 (t, $J = 8.6$ Hz, 2H, -CH₂-Ph), 2.53–2.43 (m, 4H, 2x-NCH₂- of morph), 2.30–2.26 (m, 2H, -CH₂- of morph), 2.19–2.17 (m, 2H, -CH₂-C₆H₄-Br). ^{13}C NMR (101 MHz, CDCl_3): δ 171.57 (s), 140.05 (s), 138.02 (s), 132.91 (s), 130.83 (s), 129.45 (s), 128.55 (s), 128.17 (s), 127.64 (s), 126.57 (s), 124.35 (s), 66.89 (s), 65.06 (s), 61.26 (s), 53.60 (s), 51.58 (s), 39.02 (s), 36.61 (s), 32.23 (s), 29.80 (s).

4.2.4. *N*-(3-Hydroxy-4-morpholino-1-phenylbutan-2-yl)-2-(4(trifluoromethyl)phenyl)acetamide (6c). White solid; m.p. 130–132 °C; R_f value: 0.7 (1 : 9 methanol/chloroform). Yield: 46%. ^1H NMR (400 MHz, CDCl_3): δ 7.55–7.52 (d, $J = 8.7$ Hz, 2x-CH- of -C₆H₄-CF₃), 7.26–7.22 (m, 2H, 2x-CH- of -C₆H₄-CF₃), 7.17–7.15 (m, 5H, -C₆H₅), 5.85–5.82 (d, $J = 10.0$ Hz, 1H, -OH), 4.11–4.04 (dd, $J = 18.1$, 8.7 Hz, 1H, -CH(OH)CH₂-), 3.70 (brs, 1H, -NH-CH-), 3.66–3.62 (m, 4H, 2x-OCH₂- of morph), 3.52 (s, 2H, -CH(CO)-), 2.89–2.87 (d, $J = 8.1$ Hz, 2H, -CH₂-Ph), 2.55–2.50 (m, 2H, -CH₂-morph), 2.23–2.07 (m, 4H, 2x-NCH₂- of morph). ^{13}C NMR (101 MHz, CDCl_3): δ 169.74 (s), 139.17 (s), 137.74 (s), 129.50 (s), 129.34 (s), 128.56 (s), 126.62 (s), 125.82 (s), 125.78 (s), 66.94 (s), 65.51 (s), 61.13 (s), 53.51 (s), 51.52 (s), 43.74 (s), 38.96 (s).

4.2.5. *N*-(3-Hydroxy-4-morpholino-1-phenylbutan-2-yl)-4-morpholinobenzamide (6d). White solid; m.p. 200–203 °C; R_f value: 0.3 (1 : 9 methanol/chloroform). Yield: 51%. ^1H NMR (400 MHz, CDCl_3): δ 7.69–7.67 (d, $J = 8.8$ Hz, 2H, *ortho*, 2x-COC₆H₅), 7.29–7.18 (m, 5H, -C₆H₅), 6.87–6.85 (d, $J = 8.8$ Hz, 2H, *meta*, 2x-COC₆H₅), 6.55–6.53 (d, $J = 9.2$ Hz, 1H, -OH), 4.30–4.26 (m, 1H, -CH(OH)CH₂-), 3.85–3.80 (m, 4H, 2x-OCH₂ of -C₆H₄-morph), 3.79–3.77 (d, $J = 3.1$ Hz, 1H, -NH-CH-), 3.65 (m, 4H, 2x-OCH₂ of -CH₂-morph), 3.23–3.21 (m, 4H, 2x-NCH₂ of -C₆H₄-morph), 3.05–2.99 (m, 2H, -CH₂-Ph), 2.56–2.53 (m, 2H, -CH₂-morph), 2.35–2.24 (m, 4H, 2x-NCH₂- of

morph). ^{13}C NMR (101 MHz, CDCl_3): δ 166.72 (s), 153.50 (s), 138.23 (s), 129.52 (s), 128.57 (s), 128.47 (s), 126.53 (s), 124.67 (s), 114.13 (s), 67.00 (s), 66.72 (s), 65.35 (s), 61.36 (s), 53.58 (s), 51.85 (s), 48.14 (s), 39.25 (s).

4.2.6. *N*-(3-Hydroxy-4-morpholino-1-phenylbutan-2-yl)-2-phenylpropanamide (6e). White solid; m.p. 119–121 °C; R_f value: 0.6 (1 : 9 methanol/chloroform). Yield: 55%. ^1H NMR (400 MHz, CDCl_3): δ 7.29–7.25 (m, 5H, -C₆H₅(CH)CH₃-), 7.21–7.11 (m, 5H, -C₆H₅), 5.85–5.72 (dd, $J = 40.1$, 9.3 Hz, 1H, -OH), 4.06–4.00 (dd, $J = 17.1$, 8.7 Hz, 1H, -CH(OH)CH₂-), 3.65–3.59 (d, $J = 24.4$ Hz, 5H, 2x-OCH₂- of morph + -CH(CO)), 3.52 (m, 1H, -CH-NH-), 2.87–2.78 (m, 2H, -CH₂-Ph), 2.53–2.51 (m, 2H, -CH₂- of morph), 2.25–2.06 (m, 4H, 2x-NCH₂- of morph), 1.43–1.41 (d, $J = 5.6$ Hz, 3H, -C(CH₃)). ^{13}C NMR (101 MHz, CDCl_3): δ 174.13 (s), 141.18 (s), 137.93 (s), 129.40 (s), 128.95 (s), 128.47 (s), 127.55 (s), 127.26 (s), 126.47 (s), 66.94 (s), 65.59 (s), 61.19 (s), 53.55 (s), 51.48 (s), 47.24 (s), 38.75 (s), 18.41 (s).

4.2.7. *N*-(3-Hydroxy-4-morpholino-1-phenylbutan-2-yl)-2-phenylacetamide (6f). White solid; m.p. 135–137 °C; R_f value: 0.6 (1 : 9 methanol/chloroform). Yield: 57%. ^1H NMR (400 MHz, CDCl_3): δ 7.32–7.23 (m, 5H, -C₆H₅CH₂CO-), 7.18–7.14 (m, 5H, -CH₂C₆H₅), 5.85–5.83 (d, $J = 9.3$ Hz, 1H, -OH), 4.08–4.02 (dd, $J = 17.0$, 7.8 Hz, 1H, -CH(OH)CH₂-), 3.66 (m, 1H, -CHNH-), 3.62 (m, 4H, 2x-OCH₂- of morph), 3.50–3.48 (d, $J = 4.6$ Hz, 2H, -C₆H₅CH₂CO-), 2.86–2.84 (d, $J = 8.2$ Hz, 2H, -CH₂-Ph), 2.54–2.47 (m, 2H, -CH₂-morph), 2.22–2.09 (m, 4H, 2x-NCH₂- of morph). ^{13}C NMR (101 MHz, CDCl_3): δ 170.88 (s), 137.96 (s), 135.08 (s), 129.42 (s), 129.31 (s), 129.02 (s), 128.53 (s), 127.33 (s), 126.54 (s), 66.99 (s), 65.45 (s), 61.11 (s), 53.53 (s), 51.59 (s), 44.07 (s), 38.86 (s).

4.2.8. *N*-(3-Hydroxy-4-morpholino-1-phenylbutan-2-yl)-2-(*p*-tolyl)oxy) acetamide (6g). White solid; m.p. 74–76 °C; R_f value: 0.5 (1 : 9 methanol/chloroform). Yield: 52%. ^1H NMR (400 MHz, CDCl_3): δ 7.27–7.22 (m, 4H, *ortho*, *meta* 2x -C₆H₄-), 7.09–7.02 (d, $J = 8.4$ Hz, 2H, 2x-*meta* of methoxy-C₆H₄-), 6.97–6.95 (d, $J = 9.6$ Hz, 1H, *para* -CH₂-C₆H₅), 6.80–6.78 (d, $J = 8.5$ Hz, 2H, 2x-*ortho* of methoxy-C₆H₄-), 4.48–4.37 (qt, $J = 21.4$ Hz, 2H, -OCH₂-(CO)-), 4.14–4.08 (m, 1H, -CH(OH)CH₂-), 3.73–3.69 (m, 1H, -CH-NH-), 3.67–3.60 (m, 4H, 2x-OCH₂- of morph), 2.99–2.94 (d, $J = 14.7$, 7.7 Hz, 2H, -CH₂-Ph), 2.53–2.48 (m, 2H, -CH₂- morph), 2.27 (s, 3H, CH₃-C₆H₄-), 2.24–2.16 (m, 4H, 2x-NCH₂- of morph). ^{13}C NMR (101 MHz, CDCl_3): δ 168.45 (s), 155.26 (s), 137.81 (s), 131.46 (s), 130.27 (s), 129.49 (s), 128.57 (s), 126.62 (s), 114.62 (s), 67.54 (s), 66.84 (s), 64.99 (s), 61.15 (s), 53.50 (s), 51.38 (s), 39.00 (s), 20.56 (s).

4.2.9. *N*-(3-Hydroxy-4-morpholino-1-phenylbutan-2-yl)-5-methylpyrazine-2-carboxamide (6h). White solid; m.p. 92–94 °C; R_f value: 0.6 (1 : 9 methanol/chloroform). Yield: 50%. ^1H NMR (400 MHz, CDCl_3): δ 9.20 (s, 1H, *ortho*-NCH- of pyrazine), 8.38 (s, 1H, *meta*-NCH- of pyrazine), 8.16–8.13 (d, $J = 9.7$ Hz, 1H, -CH-NH-), 7.29–7.24 (m, 4H, *ortho*, *meta* 2x -C₆H₅), 7.20–7.17 (m, 1H, *para* -C₆H₅), 4.28–4.22 (m, 1H, -CH(OH)CH₂-), 3.84–3.81 (dd, $J = 10.5$, 3.7 Hz, 1H, -CH-NH-), 3.69–3.61 (m, 5H, -OH + 2x -OCH₂- of morph), 3.06–3.04 (d, $J = 7.6$ Hz, 2H, -CH₂-Ph), 2.63 (s, 3H, -pyrazine-CH₃), 2.59–2.54 (m, 2H, -CH₂- morph),

2.39–2.28 (m, 4H, 2x-NCH₂- of morph). ¹³C NMR (101 MHz, CDCl₃): δ 163.26 (s), 157.16 (s), 143.44 (s), 142.52 (s), 141.70 (s), 137.92 (s), 129.48 (s), 128.59 (s), 126.62 (s), 66.87 (s), 65.32 (s), 61.42 (s), 53.57 (s), 52.00 (s), 39.06 (s), 21.92 (s). HRMS *m/z* calcd [M + K]⁺ for C₂₀H₂₆N₄O₃K⁺: 409.1648; found: 409.1631.

4.2.10. N-(3-Hydroxy-4-morpholino-1-phenylbutan-2-yl)-2-phenylbutanamide (6i). White solid; m.p. 112–115 °C; *R_f* value: 0.6 (1:9 methanol/chloroform). Yield: 48%. ¹H NMR (400 MHz, CDCl₃): δ 7.28–7.24 (m, 5H, -(CH)-C₆H₅), 7.22–7.10 (m, 5H, -CH₂-C₆H₅), 5.81–5.79 (dd, *J* = 9.2 Hz, 1H, -OH), 4.06 (m, 1H, -CH(OH)CH₂-), 3.61–3.59 (m, 4H, 2x -OCH₂- of morph), 3.21–3.13 (dt, *J* = 33.4, 7.5 Hz, 1H, -CH-(CO)-), 2.90–2.79 (dd, *J* = 36.7, 7.9 Hz, 2H, -CH₂-Ph), 2.56–2.39 (m, 2H, -CH₂-morph), 2.28–2.23 (m, *J* = 19.4 Hz, 1H, -CH-NH-), 2.09–2.06 (m, 4H, 2x -NCH₂- of morph), 1.83–1.71 (m, 2H, -CH₂-CH₃), 0.86–0.75 (dt, *J* = 29.6, 7.3 Hz, 3H, -CH₂-CH₃). ¹³C NMR (101 MHz, CDCl₃): δ 173.34 (s), 139.95 (s), 137.91 (s), 129.36 (s), 128.81 (s), 128.44 (s), 127.85 (s), 127.13 (s), 126.43 (s), 66.89 (s), 65.53 (s), 61.20 (s), 55.48 (s), 53.33 (s), 51.44 (s), 38.79 (s), 26.08 (s), 12.46 (s). HRMS *m/z* calcd [M + H]⁺ for C₂₄H₃₃N₂O₃: 397.2491; found: 397.2489.

4.2.11. N-(3-Hydroxy-4-morpholino-1-phenylbutan-2-yl)-4-(4-methylpiperazin-1-yl)benzamide (6j). White solid; m.p. 125–127 °C; *R_f* value: 0.7 (1:9 methanol/chloroform). Yield: 45%. ¹H NMR (400 MHz, CDCl₃): δ 7.67–7.65 (d, *J* = 8.9 Hz, 2H, *ortho*-C₆H₅-CO-), 7.30–7.25 (m, 4H, *ortho*, *meta*-C₆H₅), 7.20–7.16 (m, 1H, *para*-C₆H₅), 6.88–6.86 (d, *J* = 8.9 Hz, 2H, *meta*-C₆H₄-CO-), 6.53–6.50 (d, *J* = 9.3 Hz, 1H, -OH), 4.29–4.23 (m, 1H, -CH(OH)CH₂-), 3.79–3.75 (dd, *J* = 10.7, 3.5 Hz, 1H, -CH-NH-), 3.65–3.62 (m, 4H, 2x -OCH₂- of morph), 3.30–3.27 (m, 4H, 2x -NCH₂- of piperazine), 3.08–2.98 (m, 2H, -CH₂-Ph), 2.56–2.51 (m, 6H, 3x -NCH₂- of morph), 2.33–2.26 (m, 7H, 2x -NCH₂ of piperazine + CH₃- piperazine). ¹³C NMR (101 MHz, CDCl₃): δ 166.76 (s), 153.42 (s), 138.26 (s), 129.52 (s), 128.56 (s), 128.43 (s), 126.50 (s), 124.11 (s), 114.31 (s), 67.02 (s), 65.35 (s), 61.34 (s), 54.87 (s), 53.56 (s), 51.81 (s), 47.87 (s), 46.20 (s), 39.26 (s).

4.2.12. 3-(4-Bromophenyl)-N-(3-hydroxy-4-morpholino-1-phenylbutan-2-yl)propanamide (6k). White solid; m.p. 122–124 °C; *R_f* value: 0.4 (1:9 methanol/chloroform). Yield: 60%. ¹H NMR (400 MHz, CDCl₃): δ 7.52–7.50 (d, *J* = 7.7 Hz, 1H, -NH-), 7.26–7.18 (m, 8H, *ortho*, *meta*-C₆H₅), 7.07–7.03 (m, 1H, *para*-C₆H₅), 5.85–5.82 (d, *J* = 9.3 Hz, 1H, -OH), 4.07–4.01 (m, 1H, -CH(OH)CH₂-), 3.68–3.65 (m, 5H, -CH-NH- + -OCH₂- of morph), 3.03–2.95 (m, 2H, -CH₂-C₆H₄-Br), 2.87–2.86 (d, *J* = 7.6, 2.7 Hz, 2H, -CH₂-Ph), 2.54–2.50 (dd, *J* = 10.4, 5.4 Hz, 2H, -CH₂-morph), 2.47–2.44 (t, *J* = 7.6 Hz, 2H, -CH₂-(CO)-), 2.28–2.15 (m, 4H, 2x -NCH₂- of morph). ¹³C NMR (101 MHz, CDCl₃): δ 171.32 (s), 139.86 (s), 137.95 (s), 131.58 (s), 130.38 (s), 129.42 (s), 128.55 (s), 126.59 (s), 120.11 (s), 66.95 (s), 64.92 (s), 61.10 (s), 53.59 (s), 51.42 (s), 39.09 (s), 38.20 (s), 30.89 (s). HPLC Purity: 97.6%.

4.2.13. 4-Fluoro-N-(3-hydroxy-4-morpholino-1-phenylbutan-2-yl)benzamide (6l). White solid; m.p. 164–169 °C; *R_f* value: 0.3 (1:9 methanol/chloroform). Yield: 40%. ¹H NMR (400 MHz, CDCl₃): δ 7.75–7.72 (m, 2H, *ortho*-C₆H₄-F), 7.29–7.28 (d, *J* = 12.4, 3.7 Hz, 4H, *ortho*, *meta*-C₆H₅), 7.22–7.19 (m, 1H, *para*

-C₆H₅), 7.11–7.07 (m, 2H, *meta*-C₆H₄-F), 6.59–6.57 (d, *J* = 9.2 Hz, 1H, -OH), 4.30–4.24 (m, 1H, -CH(OH)CH₂-), 3.82–3.78 (dd, *J* = 10.4, 3.8 Hz, 1H, -CH-NH-), 3.69–3.62 (m, 4H, 2x -OCH₂- of morph), 3.09–2.98 (m, 2H, CH₂-Ph), 2.59–2.54 (m, 2H, -CH₂-morph), 2.36–2.28 (m, 4H, 2x -NCH₂- of morph). ¹³C NMR (101 MHz, CDCl₃): δ 166.13 (s), 163.57 (s), 137.96 (s), 129.48 (s), 129.34 (s), 129.25 (s), 128.61 (s), 126.64 (s), 115.80 (s), 66.98 (s), 65.31 (s), 61.38 (s), 53.58 (s), 52.08 (s), 39.19 (s).

4.2.14. N-(3-Hydroxy-4-morpholino-1-phenylbutan-2-yl)-4-(trifluoromethyl)benzamide (6m). White solid; m.p. 162–165 °C; *R_f* value: 0.3 (1:9 methanol/chloroform). Yield: 44%. ¹H NMR (400 MHz, CDCl₃): δ 7.83–7.81 (d, *J* = 4.3 Hz, 2H, *ortho*-C₆H₄-CF₃), 7.69–7.67 (d, *J* = 8.4 Hz, 2H, *meta*-C₆H₄-CF₃), 7.30–7.28 (m, 4H, *ortho*, *meta*-C₆H₅), 7.25–7.21 (m, 1H, *para*-C₆H₅), 6.68–6.66 (d, *J* = 9.3 Hz, 1H, -OH), 4.32–4.26 (qt, *J* = 16.4 Hz, 1H, -CH(OH)CH₂-), 3.68–3.67 (m, 1H, -CH-NH-), 3.65–3.64 (m, 4H, 2x -OCH₂- of morph), 3.09–3.03 (m, 2H, -CH₂-Ph), 2.60–2.55 (m, 2H, -CH₂-morph), 2.39–2.30 (m, 4H, 2x -NCH₂- of morph). ¹³C NMR (101 MHz, CDCl₃): δ 165.91 (s), 137.79 (s), 133.79 (s), 133.49 (s), 133.16 (s), 129.47 (s), 128.65 (s), 127.46 (s), 126.73 (s), 125.75 (s), 125.71 (s), 66.99 (s), 65.28 (s), 61.35 (s), 53.58 (s), 52.16 (s), 39.19 (s).

4.3. Parasite culture

The chloroquine-sensitive (CQ^S) (3D7) *P. falciparum* strain was cultured in freshly collected donor erythrocytes in a complete RPMI-based malaria culture medium (CMCM) according to the Malaria Research and Reference Reagent Resource Center (MR4) guidelines.⁵¹ Thin blood smears stained with Giemsa were prepared for routine monitoring. Synchronized culture (trophozoites) was taken for the growth progression assay. To establish the morphological changes in the parasite, a blood film must be prepared. A thin film was air-dried and fixed with methanol. Blood films were stained with a 7.5% Giemsa solution (pH of 7.2) for 15 min. Parasitemia was counted using a brightfield microscope, and the morphological changes were noted *via* imaging.

4.4. Cytotoxicity effects of compounds on normal human cells

Cytotoxicity against human cell lines (HepG2) was determined using MTT dye. HepG2 was maintained at 37 °C, 5% CO₂ in sterile culture flasks, and complete DMEM medium supplemented with 5% FBS, and gentamicin (40 mg mL⁻¹). Media were refreshed thrice a week. The cells were trypsinized (0.05% trypsin/0.5 mM EDTA), washed, and distributed in 96-well plates (5000 cells per well), followed by incubation for another 24 h at 37 °C. The test compounds and DMSO were added in triplicate. After 3 h of incubation at 37 °C, the supernatant was removed and 100 μL fresh media were added and the kept plates in an incubator at 37 °C, then 100 μL of the MTT solution in complete DMEM was added to each well after 24, 48, and 72 h of incubation. The culture plates were read at 570 nm in a spectrophotometer (Tecan Infinite M200, Nanoquant, UK) with a 490 nm filter at different time points. To determine cytotoxic concentrations, a dose-response curve was prepared.

4.5. Hemolysis assay

Hemolysis assay was performed using RBCs suspension 10% (v/v) washed with $1 \times$ PBS (pH 7.4) and resuspended in $1 \times$ PBS. The suspension was treated with compounds at different concentrations for 2 hours at 37 °C. Samples were centrifuged at $800 \times g$ for 5 min at room temperature. The supernatant was taken for absorbance at 540 nm to obtain the percentage of RBCs lysis. Triton X-100 with 0.1% (v/v) was used as a positive control. The percentage of RBCs lysis was obtained by using the following formula:

$$\% \text{ RBCs lysis} = \frac{(\text{OD}_{500\text{nm}} \text{ sample} - \text{OD}_{500\text{nm}} \text{ PBS})}{(\text{OD}_{500\text{nm}} \text{ Triton X-100 0.1\%} - \text{OD}_{500\text{nm}} \text{ PBS})}$$

4.6. *In vitro* drug combination experiment

The *in vitro* combination assay was done using ART and **6k** at different concentrations. A 24-well plate was used to perform the assay and was incubated for 48 hours at 37 °C. After that, thin blood smears were drawn and stained with a buffer solution of the Giemsa stain (9 : 1). The slides with smears were read with a 100X immersion oil lens of the brightfield microscope.

4.7. Stage-specific study

Parasite cultures with 80% trophozoites, 18% rings, and 2% schizonts were obtained by synchronization with 5% sorbitol. The assay was performed in a 24 well microtiter plate with a 2-fold dilution of culture, and the IC_{50} drug concentrations of 5 μM (**6k**) and 3 nM (ART) were used. The plate was incubated for 50 hours at 37 °C. The parasitemia was calculated using Giemsa-stained thin blood smears.⁵²

4.8. *In vitro* activity against *P. berghei* hepatic (liver) stages

In vitro activity against the liver stage of *P. berghei* infection was assessed as previously described.^{53,54} Briefly, Huh7 cells were routinely cultured in 1640 Roswell Park Memorial Institute (RPMI) medium supplemented with 10% (v/v) fetal bovine serum, 1% (v/v) glutamine, 1% (v/v) penicillin/streptomycin, 1% non-essential amino acids, and mM 2-(4-(2-hydroxyethyl)-piperazin-1-yl)ethanesulfonic acid (HEPES). For drug screening experiments, Huh7 cells were seeded in 96-well plate and incubated overnight at 37 °C with 5% CO_2 . The stock solutions of the test compounds were prepared in DMSO and were serially diluted in an infection medium, *i.e.*, culture medium supplemented with gentamicin (50 mg mL^{-1}) to get the test concentrations. On the day of the infection, the culture medium was replaced by the serial dilutions of test compounds and incubated for 1 h at 37 °C with 5% CO_2 . Next, firefly luciferase-expressing *P. berghei* sporozoites, freshly isolated from the salivary glands of female infected *Anopheles* mosquitoes, were added to the cultures, and the plates were centrifuged at $1800g$ for 5 min at room temperature and incubated at 37 °C with 5% CO_2 . To assess the effect of each compound concentration on the cell viability, at 46 h post-infection (hpi), cultures were incubated with Alamar Blue,

according to the manufacturer's recommendations. Parasite load was then assessed by a bioluminescence assay using a multi-plate reader. Nonlinear regression analysis was employed to fit the normalized results of the dose-response curves, and IC_{50} values were determined using GraphPad Prism 6.0 (GraphPad software).

4.9. Recombinant *PfPlm X* activity assay

Protease cleavage assays were performed with purified recombinant PMX in digestion buffer (25 mM Tris-HCl, 25 mM MES, pH 6.4 and 5.5 for PMX), respectively; 0.2 μM of a synthetic peptide substrate (ThermoFisher scientific, >98% purity). Samples were incubated at 37 °C for 1 hour and the fluorescence was measured using a SynergyH1 multi-well plate reader (BioTek) excited at 340 nm and reading emissions at 490 nm. Samples were gently shaken during incubation. Changes in Relative Fluorescence Units (RFU) were measured for each time point by subtracting the RFU from the blank (without enzyme) for each time point.⁴³

4.10. Computational

4.10.1. Homology modelling and structure validation. The PlmX structure was modeled using the Swiss model tool (<https://swissmodel.expasy.org/>). [Cathepsin D of *Rattus norvegicus* (Rat)] was taken as a template for PlmX structure modeling. The stereochemical geometry of PlmX residues was measured by the Ramachandran map (By Procheck). The computational work was performed using Schrodinger software (Schrodinger release 2020-1 license dated 20 November 2020).

4.10.2. Preparation of the protease structure and active site identification. The preparations of the modeled structure and molecular library, molecular docking, and molecular dynamic simulation were done as per the literature.⁵⁵ The OPLS2005 forcefield was used in this *in silico* study. Residues involved in the binding site were predicted through the CastP server.⁵⁶

4.10.3. ADME profile. ADME-related properties for the designed **6k** compound were calculated using SwissADME. Molecular weight (M_w), number of rotatable bonds, number of H-bond acceptors, number of H-bond donors, octanol/water partition coefficient ($M\text{Log}P$), the logarithm of water solubility (ESOL $\text{Log}S$), *etc.* were calculated. Other predicted properties were GI absorption tendency, BBB permeability behavior, and Lipinski rule.

Abbreviations

ABS	Asexual blood-stage
ACT	Artemisinin-based combination therapy
ADME	Absorption, distribution, metabolism, excretion
BOC	<i>Tert</i> -butyloxycarbonyl
DCM	Dichloromethane
EDC-HCL	1-(3-Dimethylaminopropyl)-3-ethylcarbodiimide hydrochloride
HEA	Hydroxyethylamine

HEPES	(4-(2-Hydroxyethyl)-1-piperazineethanesulfonic acid)
HPLC	High-performance liquid chromatography
RBC	Red blood cells
HRMS	High-resolution mass spectrometry
IC ₅₀	Half-maximal inhibitory concentration; MD, molecular dynamics
NMR	Nuclear magnetic resonance
<i>P. berghei</i>	Plasmodium berghei
PBS	Phosphate-buffered saline
<i>Pf</i>	<i>Plasmodium falciparum</i>
Plm	Plasmepsin
PQ	Primaquine
RMSD	Root-mean-squared deviation
SAR	Structure–activity relationship
TC ₅₀	50% cytotoxic concentration
TFA	Trifluoroacetic acid
TLC	Thin-layer chromatography
WHO	World Health Organization.

Author contributions

Conceptualization, C. U., D. K., M. P., A. P. S, Poonam.; methodology, C. U., N. S., S. K, P. P. S., D. F., B. M., B. S. C and D. K.; writing—original draft preparation, C. U., A. P. S. and Poonam; writing—review and editing, C. U., B. S. C, D. K., M. P., A. P. S. and Poonam.; supervision, project administration, and funding acquisition, Poonam. All authors have read and agreed to the published version of the manuscript.

Conflicts of interest

Authors declare no conflict of interest.

Acknowledgements

Poonam acknowledges Science and Engineering Research Board for financial support under CRG scheme (CRG/2020/005800). CU, NS and SK are highly grateful to CSIR for senior research fellowship, PPS acknowledges DBT, Govt. of India for senior research fellowship.

References

- N. Sharma, A. Verma, P. Fnu, P. Kempaiah and B. Rathi, *Chem. Biol. Lett.*, 2019, **6**, 14–22.
- N. M. Pazhayam, J. Chhibber-Goel and A. Sharma, *Drug Discovery Today*, 2019, **24**, 263–271.
- S. Rout and R. K. Mahapatra, *Chem. Biol. Drug Des.*, 2019, **93**, 737–759.
- N. D. Pasternak and R. Dzikowski, *Int. J. Biochem. Cell Biol.*, 2009, **41**, 1463–1466.
- World Health Organization: World malaria report 2020, <https://www.who.int/publications/i/item/9789240015791>, accessed march 22, 2021.
- E. G. Tse, M. Korsik and M. H. Todd, *Malar. J.*, 2019, **18**, 93.
- Poonam, Y. Gupta, N. Gupta, S. Singh, L. Wu, B. S. Chhikara, M. Rawat and B. Rathi, *Med. Res. Rev.*, 2018, **38**, 1511–1535.
- K. Halder, S. Bhattacharjee and I. Safeukui, *Nat. Rev. Microbiol.*, 2018, **16**, 156–170.
- N. Sharma, Y. Gupta, M. Bansal, S. Singh, P. Pathak, M. Shahbaaz, R. Mathur, J. Singh, M. Kashif, M. Grishina, V. Potemkin, V. Rajendran, Poonam, P. Kempaiah, A. P. Singh and B. Rathi, *RSC Adv.*, 2020, **10**, 35516–35530.
- M. A. Diallo, M. S. Yade, Y. D. Ndiaye, I. Diallo, K. Diongue, S. A. Sy, M. Sy, M. C. Seck, M. Ndiaye, B. Dieye, J. F. Gomis, D. Sow, A. B. Dème, A. S. Badiane and D. Ndiaye, *Sci. Rep.*, 2020, **10**, 8907.
- J. E. Hyde, *FEBS J.*, 2007, **274**, 4688–4698.
- K. S. Griffith, L. S. Lewis, S. Mali and M. E. Parise, *JAMA*, 2007, **297**, 2264–2277.
- C. Upadhyay, M. Chaudhary, R. N. De Oliveira, A. Borbas, P. Kempaiah, Poonam and B. Rathi, *Expert Opin. Drug Discovery*, 2020, **15**, 705–718.
- J. Achan, J. Mwesigwa, C. P. Edwin and U. D'alessandro, *Expert Rev. Clin. Pharmacol.*, 2018, **11**, 61–70.
- S. Yahiya, A. Rueda-Zubiaurre, M. J. Delves, M. J. Fuchter and J. Baum, *Curr. Opin. Chem. Biol.*, 2019, **50**, 1–9.
- M. Al-Ghorbani, B. A. Bushra, S. Mamatha and S. A. Khanum, *Res. J. Pharm. Technol.*, 2015, **8**, 611–628.
- M. Asif and M. Imran, *Frontiers in Chemical Research*, 2019, **1**, 5–12.
- K. Rupak, S. R. Vulichi and K. Suman, *Int. J. Chem. Sci.*, 2016, **14**, 1777–1788.
- F. Arshad, M. F. Khan, W. Akhtar, M. M. Alam, L. M. Nainwal, S. K. Kaushik, M. Akhter, S. Parvez, S. M. Hasan and M. Shaquiquzzaman, *Eur. J. Med. Chem.*, 2019, **167**, 324–356.
- A. P. Kourounakis, D. Xanthopoulos and A. Tzara, *Med. Res. Rev.*, 2020, **40**, 709–752.
- E. A. Ashley and A. P. Phyto, *Drugs*, 2018, **78**, 861–879.
- B. Rathi, A. K. Singh, R. Kishan, N. Singh, N. Latha, S. Srinivasan, K. C. Pandey, H. K. Tiwari and B. K. Singh, *Bioorg. Med. Chem.*, 2013, **21**, 5503–5509.
- M. C. Souza, T. A. Padua, N. D. Torres, M. F. D. S. Costa, V. Facchinetti, C. R. B. Gomes, M. V. N. Souza and M. D. G. Henriques, *Mem. Inst. Oswaldo Cruz*, 2015, **110**, 560–565.
- P. P. Sharma, S. Kumar, K. Kaushik, A. Singh, I. K. Singh, M. Grishina, K. C. Pandey, P. Singh, V. Potemkin, Poonam, G. Singh and B. Rathi, *J. Biomol. Struct. Dyn.*, 2021, 1–13.
- N. Sharma, M. Kashif, V. Singh, D. Fontinha, B. Mukherjee, D. Kumar, S. Singh, M. Prudencio, A. P. Singh and B. Rathi, *J. Med. Chem.*, 2021, **64**, 8666–8683.
- K. Jaudzems, K. Tars, G. Maurops, N. Ivdra, M. Otikovs, J. Leitans, I. Kanepe-Lapsa, I. Domraceva, I. Mutule, P. Trapencieris, M. J. Blackman and A. Jirgensons, *ACS Med. Chem. Lett.*, 2014, **5**, 373–377.
- S. Singh, V. Rajendran, J. He, A. K. Singh, A. O. Achieng, Vandana, A. Pant, A. S. Nasamu, M. Pandit, J. Singh,

- A. Quadiri, N. Gupta, Poonam, P. C. Ghosh, B. K. Singh, L. Narayanan, P. Kempaiah, R. Chandra, B. M. Dunn, K. C. Pandey, D. E. Goldberg, A. P. Singh and B. Rathi, *ACS Infect. Dis.*, 2019, 5, 184–198.
- 28 A. Kumari and R. K. Singh, *Bioorg. Chem.*, 2020, 96, 103578.
- 29 S. Kumar, Y. Gupta, S. E. Zak, C. Upadhyay, N. Sharma, A. S. Herbert, R. Durvasula, V. Potemkin, J. M. Dye, Poonam, P. Kempaiah and B. Rathi, *RSC Med. Chem.*, 2021, 12, 1757–1764.
- 30 Y. Gupta, S. Kumar, S. E. Zak, K. A. Jones, C. Upadhyay, N. Sharma, S. A. Azizi, R. S. Kathayat, Poonam, A. S. Herbert, R. Durvasula, B. C. Dickinson, J. M. Dye, B. Rathi and P. Kempaiah, *Bioorg. Med. Chem.*, 2021, 47, 116393.
- 31 S. Kumar, C. Upadhyay, M. Bansal, M. Grishina, B. S. Chhikara, V. Potemkin, B. Rathi and Poonam, *ACS Omega*, 2020, 5, 18746–18757.
- 32 F. Moschona, I. Savvopoulou, M. Tsitopoulou, D. Tataraki and G. Rassias, *Catalysts*, 2020, 10, 1117.
- 33 L. Shi, L. Chen, R. Chen and L. Chen, *J. Labelled Compd. Radiopharm.*, 2010, 53, 147–151.
- 34 W. Cunico, C. R. B. Gomes, M. Moreth, D. P. Manhanini, I. H. Figueiredo, C. Penido, M. G. M. O. Henriques, F. P. Varotti and A. U. Krettli, *Eur. J. Med. Chem.*, 2009, 44, 1363–1368.
- 35 S. Hartwig, M. M. Nguyen and S. Hecht, *Polym. Chem.*, 2010, 1, 69–71.
- 36 L. Tilley, J. Straimer, N. F. Gnädig, S. A. Ralph and D. A. Fidock, *Trends Parasitol.*, 2016, 32, 682–696.
- 37 B. Baragaña, I. Hallyburton, M. C. S. Lee, N. R. Norcross, R. Grimaldi, T. D. Otto, W. R. Proto, A. M. Blagborough, S. Meister, G. Wirjanata, A. Ruecker, L. M. Upton, T. S. Abraham, M. J. Almeida, A. Pradhan, A. Porzelle, T. Luksch, M. S. Martínez, T. Luksch, J. M. Bolscher, A. Woodland, S. Norval, F. Zuccotto, J. Thomas, F. Simeons, L. Stojanovski, M. Osuna-Cabello, P. M. Brock, T. S. Churcher, K. A. Sala, S. E. Zakutansky, M. B. Jiménez-Díaz, L. M. Sanz, J. Riley, R. Basak, M. Campbell, V. M. Avery, R. W. Sauerwein, K. J. Dechering, R. Noviyanti, B. Campo, J. A. Frearson, I. Angulo-Barturen, S. Ferrer-Bazaga, F. J. Gamó, P. G. Wyatt, D. Leroy, P. Siegl, M. J. Delves, D. E. Kyle, S. Wittlin, J. Marfurt, R. N. Price, R. E. Sinden, E. A. Winzeler, S. A. Charman, L. Bebrevska, D. W. Gray, S. Campbell, A. H. Fairlamb, P. A. Willis, J. C. Rayner, D. A. Fidock, K. D. Read and I. H. Gilbert, *Nature*, 2015, 522, 315–320.
- 38 M. Prudêncio, M. M. Mota and A. M. Mendes, *Trends Parasitol.*, 2011, 27, 565–574.
- 39 R. Raphemot, D. Posfai and E. R. Derbyshire, *J. Clin. Invest.*, 2016, 126, 2013–2020.
- 40 I. M. Vera, M. T. G. Ruivo, L. F. L. Rocha, S. Marques, S. N. Bhatia, M. M. Mota and L. Mancio-Silva, *JCI Insight*, 2019, 4, e127441.
- 41 A. O. da Silva de Barros, F. L. Portilho, A. P. dos Santos Matos, E. Ricci-Junior, L. M. R. Alencar, C. C. dos Santos, F. J. R. Paumgartten, S. H. Iram, D. Mazier, J.-F. Franetich, F. Alexis and R. Santos-Oliveira, *Mater. Sci. Eng., C*, 2021, 128, 112275.
- 42 T. Rodrigues, M. Prudêncio, R. Moreira, M. M. Mota and F. Lopes, *J. Med. Chem.*, 2012, 55, 995–1012.
- 43 P. Pino, R. Caldelari, B. Mukherjee, J. Vahokoski, N. Klages, B. Maco, C. R. Collins, M. J. Blackman, I. Kursula, V. Heussler, M. Brochet and D. Soldati-Favre, *Science*, 2017, 358, 522–528.
- 44 G. Munsamy, P. Ramharack and M. E. S. Soliman, *RSC Adv.*, 2018, 8, 21829–21840.
- 45 J. N. Burrows and D. Soldati-Favre, *Cell Host Microbe*, 2020, 27, 496–498.
- 46 A. S. Nasamu, S. Glushakova, I. Russo, B. Vaupel, A. Oksman, A. S. Kim, D. H. Fremont, N. Tolia, J. R. Beck, M. J. Meyers, J. C. Niles, J. Zimmerberg and D. E. Goldberg, *Science*, 2017, 358, 518.
- 47 A. Kumar Singh, V. Rajendran, S. Singh, P. Kumar, Y. Kumar, A. Singh, W. Miller, V. Potemkin, Poonam, M. Grishina, N. Gupta, P. Kempaiah, R. Durvasula, B. K. Singh, B. M. Dunn and B. Rathi, *Bioorg. Med. Chem.*, 2018, 26, 3837–3844.
- 48 D. E. Goldberg, *Curr. Top. Microbiol. Immunol.*, 2005, 295, 275–291.
- 49 B. Baragaña, N. R. Norcross, C. Wilson, A. Porzelle, I. Hallyburton, R. Grimaldi, M. Osuna-Cabello, S. Norval, J. Riley, L. Stojanovski, F. R. Simeons, P. G. Wyatt, M. J. Delves, S. Meister, S. Duffy, V. M. Avery, E. A. Winzeler, R. E. Sinden, S. Wittlin, J. A. Frearson, D. W. Gray, A. H. Fairlamb, D. Waterson, S. F. Campbell, P. Willis, K. D. Read and I. H. Gilbert, *J. Med. Chem.*, 2016, 59, 9672–9685.
- 50 A. K. Singh, S. Rathore, Y. Tang, N. E. Goldfarb, B. M. Dunn, V. Rajendran, P. C. Ghosh, N. Singh, N. Latha and B. K. Singh, *PLoS One*, 2015, 10, e0139347.
- 51 F. Mphande, S. Nilsson and A. Bolad, *Methods in malaria research*, 2008, 1.2008, 1.
- 52 S. Duffy and V. M. Avery, *Int. J. Parasitol.: Drugs Drug Resist.*, 2017, 7, 295–302.
- 53 B. Pérez, C. Teixeira, I. S. Albuquerque, J. Gut, P. J. Rosenthal, M. Prudêncio and P. Gomes, *MedChemComm*, 2012, 3, 1170–1172.
- 54 F. P. da Cruz, C. Martin, K. Buchholz, M. J. Lafuente-Monasterio, T. Rodrigues, B. Sönnichsen, R. Moreira, F.-J. Gamó, M. Marti, M. M. Mota, M. Hannus and M. Prudêncio, *J. Infect. Dis.*, 2012, 205, 1278–1286.
- 55 S. Kumar, P. P. Sharma, U. Shankar, D. Kumar, S. K. Joshi, L. Pena, R. Durvasula, A. Kumar, P. Kempaiah, Poonam and B. Rathi, *J. Chem. Inf. Model.*, 2020, 60, 5754–5770.
- 56 W. Tian, C. Chen, X. Lei, J. Zhao and J. Liang, *Nucleic Acids Res.*, 2018, 46, W363–W367.